Available online at www.sciencedirect.com
ScienceDirect
C. R. Physique 10 (2009) 514–527
COMPTES RENDUS PHYSIQUE
http://france.elsevier.com/direct/COMREN/

Theoretical spectroscopy / Spectroscopie théorique

Local atomic order and optical properties in amorphous and laser-crystallized GeTe

Wojciech Wełnic [a,b,c,*], Matthias Wuttig [c], Silvana Botti [a,b,d], Lucia Reining [a,b]

[a] *Laboratoire des solides irradiés, CNRS-CEA, École polytechnique, 91128 Palaiseau cedex, France*
[b] *European Theoretical Spectroscopy Facility (ETSF)*
[c] *I. Physikalisches Institut IA, RWTH Aachen University, 52066 Aachen, Germany*
[d] *LPMCN, Université Claude-Bernard Lyon I and CNRS, 69622 Villeurbanne, France*

Available online 5 December 2008

Abstract

In this work we study the role of short-range order changes upon amorphization on the optical properties of GeTe – a prototype phase change material employed for optical data storage. It is found that the profound change in the absorption is due to changes in the matrix elements of the optical transitions. The importance of the local distortions in the crystalline phase for the optical absorption are revealed as well. Modifying the degree of the distortions has a significant impact on the optical properties of the crystalline state and should therefore become a promising instrument to improve material properties for storage applications.

Furthermore we study the effect of electron–electron and electron–hole interactions on the optical properties. This is achieved by evaluating many-body effects in the crystalline phase through a *GW* correction of eigenvalues and the solution of the Bethe–Salpeter equation. ***To cite this article: W. Wełnic et al., C. R. Physique 10 (2009).***

Résumé

L'ordre local et des propriétés optiques de GeTe amorphe et cristalin. Dans cet article, nous étudions l'influence du changement de l'ordre à courte portée pendant l'amorphisation sur les propriétés optiques de GeTe. Cet alliage est un matériau à changement de phase typique, employé dans le stockage de données optiques. On trouve que la modification important de l'absorption vient du changement des éléments de matrice des transitions optiques. L'influence des distorsions locales dans l'état cristallin sur l'absorption optique est aussi mis en évidence. En modifiant l'amplitude des distorsions par des variations de stoechiométrie, les propriétés optiques changent. Cet effet peut être exploité pour optimiser les propriétés de ces matériaux.

En outre nous étudions l'effet des interactions électron–électron et électron–trou sur les propriétés optiques par une analyse des effets à *N* corps dans l'état cristallin. Nous examinons les corrections aux valeurs propres dans l'approximation *GW* et la solution de l'équation Bethe–Salpeter. ***Pour citer cet article : W. Wełnic et al., C. R. Physique 10 (2009).***

Keywords: Phase change materials; Electronic structure calculations; RPA

Mots-clés : Matériaux avec changement de phase ; Calculs des structures électroniques ; RPS

* Corresponding author at: Laboratoire des solides irradiés, CNRS-CEA, École polytechnique, 91128 Palaiseau cedex, France.
E-mail addresses: wojciech.welnic@polytechnique.edu (W. Wełnic), wuttig@physik.rwth-aachen.de (M. Wuttig), silvana.botti@polytechnique.edu (S. Botti), lucia.reining@polytechnique.fr (L. Reining).

1631-0705/$ – see front matter
doi:10.1016/j.crhy.2008.09.002

1. Introduction

In most covalent alloys such as GaAs the optical contrast between the crystalline and amorphous phase is reported to be comparatively small [1–3]. This is mainly attributed to the fact that the short range order, which determines the optical properties in covalently bonded materials, remains nearly unchanged [4]. This behavior is in line with the commonly used model for the amorphous phase in semiconductors, the continuous random network introduced by Zachariasen in 1932 [5]. According to this model the amorphous phase lacks the long range order which is found in the crystalline phase, but each atom is able to adopt its preferred number of bonds to the nearest neighbors as found in the crystalline state. However, for ternary GeSbTe alloys such as $Ge_2Sb_2Te_5$ and also for GeTe it has been recently observed that the local order changes upon amorphization. Using EXAFS measurements as well as first principles calculations it has been shown that the local structure around Ge atoms changes from a sixfold coordination in the crystalline state to a fourfold coordination in the amorphous state. Based upon an analysis of EXAFS data Kolobov et al. [6,7] concluded that the Ge atoms in the amorphous phase possess a tetrahedral environment and are fourfold coordinated. Using *ab initio* methods the total energy of a similar atomic arrangement, i.e. a spinel structure has been calculated. It has been found to be very similar in energy compared with the rocksalt-like structure [8]. This supports the notation that Ge atoms could indeed occupy a tetrahedral atomic arrangement in the amorphous state. Subsequent EXAFS analyses and further experimental studies [9,10] have stressed the significance of Ge–Ge bonds in the amorphous state. Recent molecular dynamics simulations provide a more detailed picture of the local order in the amorphous phase. They show that the system contains a mixture of both, octahedrally as well as tetrahedrally coordinated Ge atoms [11,12].

One of the most interesting questions in the field of these so-called Phase-Change Materials (PCM) concerns their optical properties and the link of the latter to the underlying geometrical structure. They exhibit a significant optical contrast – a change of optical reflectivity upon the phase transition from the amorphous to the crystalline state [13–15]. This property change is fundamental for the application of PCM's in optical data storage, in particular in rewritable storage devices such as DVD-RW's or, since recently, rewritable Blu-Ray discs. In this work we provide an extensive study of the optical properties in PCM's employing *ab initio* calculations within the Random Phase Approximation (RPA). We review the origin of the optical contrast between the amorphous and crystalline state and reveal the role of the local structural distortions in the crystalline state. It was recently reported that PCM's show local distortions in the crystalline rocksalt phase [6,8] which lead to the formation of short and long bonds in the crystal. The strength of these distortions depends on the stoichiometry and thus can be adjusted by systematic selection of the material [16]. Therefore, it is also of interest to study the effect of these distortions in the crystalline phase on the optical properties. A significant correlation of the absorption and the local distortions would allow for a systematic adjustment or enhancement of the optical contrast, which is of considerable commercial importance. In this work we have thus studied the effect of these distortions and compared the optical properties of a relaxed (distorted) and a non-relaxed (undistorted) crystal.

Furthermore, we study the role of electron–electron and electron–hole interactions for the optical absorption in the crystalline phase. This requires a treatment beyond the RPA as presented in [17]. Therefore we have performed *ab initio* excited state calculations within Many Body Perturbation Theory (MBPT) in order to reveal the importance of these effects on the optical properties of PCM's.

We chose GeTe for our calculations because, in contrast, to ternary phase-change alloys such as $Ge_2Sb_2Te_5$ or $Ge_1Sb_2Te_4$, its simple binary composition allows one to carry out the quite cumbersome electronic structure calculation up to a high level of precision. This also enables a detailed analysis of the differences between different structural models and different approximations.

2. Structural models

The crystalline structure of GeTe has been studied in detail. For high temperatures (above 670 K) GeTe is reported to crystallize in a sixfold coordinated cubic rocksalt phase. In the ground state at lower temperatures it adopts a trigonal phase, which can be described as a rocksalt structure, slightly distorted by freezing in a TO-phonon along the [111]-direction (see e.g. [18]). However, the reversible phase transition which is crucial for the application in optical data

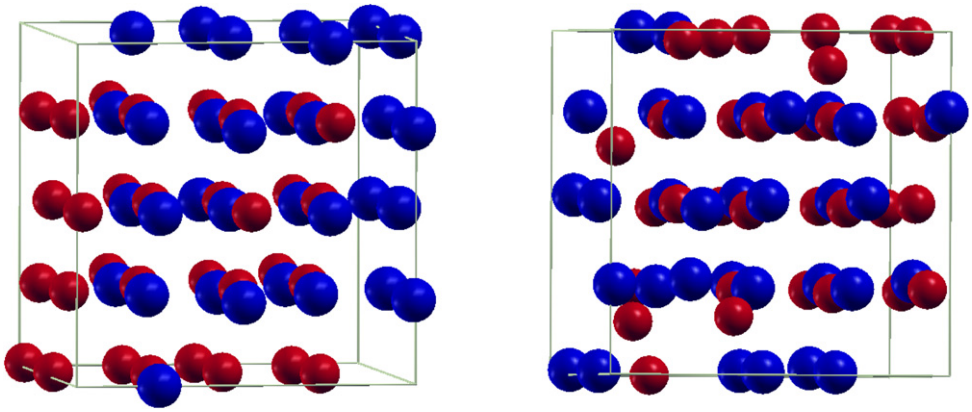

Fig. 1. Relaxed structures of the crystalline rocksalt phase (left) and of one of the amorphous models named switch4.1 (right). Ge atoms are shown in red, Te in blue.

storage takes place between the crystalline rocksalt phase and the amorphous phase. Therefore we use the rocksalt structure for the calculations of the crystalline phase. In order to study whether GeTe exhibits similar distortions in the crystalline phase as recently reported for $Ge_2Sb_2Te_5$ and $Ge_1Sb_2Te_4$ [6,8], we relax the rocksalt crystal. Within a supercell containing 64 atoms several starting configurations for a distorted rocksalt structure are chosen. Here the atoms are randomly displaced from the perfect lattice positions by 5% of the bond length. Then a relaxation of the interatomic forces is performed, the ground state energy and the distribution of long and short bonds are studied. The relaxed structure is shown in Fig. 1 (left).

In the amorphous phase Ge atoms are reported to switch from octahedrally coordinated to tetrahedrally coordinated sites [7]. Obviously in GeTe this cannot hold true for all germanium atoms. As a fourfold tetrahedral coordination requires a larger volume than an octahedral coordination, a rearrangement of all Ge-atoms would lead to a volume increase of more than 30%. Experimentally volume changes upon amorphization between 6 and 10% are measured [19–21]. In [7] the coordination number for Ge is reported to be 3.3 ± 0.3. We assume a coordination number of three within the octahedral local order (with three short and three long bonds) and four within the tetrahedral short range order. Here the length of the tetrahedral bonds corresponds to the length of the short bonds in the octahedral coordination [6]. Only those are taken into account to determine the coordination number. Under these conditions one finds that a fraction of 0–60% of the Ge atoms change their short range order upon amorphization. Taking into account all short bonds a fraction of 0% corresponds to 3 nearest neighbors as in the trigonal crystalline state, while a fraction of 60% corresponds to 3.6 nearest neighbors with 40% of the Ge atoms remaining threefold coordinated and 60% changing to tetrahedrally coordinated positions. Based on these data simple structural models are obtained for the amorphous phase. In a supercell containing 64 atoms (32 Ge and 32 Te atoms) in octahedral coordination 2, 4 and 8 Ge atoms are arranged in tetrahedrally coordinated positions in order to obtain different models with different fractions of switched Ge atoms. Furthermore two different arrangements are chosen for the case that 4 Ge-atoms change their coordination: in the first, two of the Ge atoms in tetrahedral positions have one Te atom as a common nearest neighbor, in the second model, Ge atoms in tetrahedral positions do not have nearest neighbors in common. The fraction of Ge atoms in positions with tetrahedral short range order in these models corresponds to 6.25%, 12.5% and 25%, respectively. In the following we will refer to these models as switch2, switch4.0 (no nearest neighbor in common), switch4.1 (one nearest neighbor in common, shown in Fig. 1 (right)) and switch8. These simple structural models are still periodic and thus exhibit long range order which is not present in the amorphous phase. Thus changes in the optical properties which are caused by changes in the long range order will not be taken into account. However, as the wave functions of the valence bands in covalent materials are mainly localized along the interatomic bonds, the optical properties are primarily determined by the nearest-neighbor interaction. In order to study the correlation between the local atomic order and the change in optical properties upon amorphization this model is therefore well justified.

3. Computational methods

3.1. Electronic ground state calculations

Ground state calculations are performed using DFT as implemented in the ABINIT code [22],[1] which is based on pseudopotentials and a plane wave basis. Hamman-type norm-conserving pseudopotentials are generated with the FHI98PP code [23]. For germanium the 4s and 4p states and for tellurium the 5s and 5p states have been considered as valence states in the construction of the pseudopotentials, while the Ge 3d and Te 4d levels have been considered as core states. The cutoff radii r^c of the non-local components beyond which the pseudo and the all-electron eigenstates have the same energies and the same density have been set to 1.6 Bohr for the Ge 4s orbital, 2.1 Bohr for the Ge 4p orbital, 1.9 Bohr for the Te 5s orbital and 2.3 Bohr for the Te 5p orbital. The Ge 4d and Te 5d have been chosen as the local components with a cutoff radius of 1.93 and 1.52 Bohr respectively. All calculations are performed within the Generalized Gradient Approximation (GGA) for the exchange-correlation potential in the Perdew–Burke–Ernzerhof parametrization [24].

In the perfect crystalline phase we used a $8 \times 8 \times 8$ Monkhorst–Pack-grid for k-space summation. In case of the use of supercells, the integration over the Brillouin zone was performed at the Γ and L points. It was found by Makov et al. that this k-point set represents an efficient choice for simple cubic supercells [25] and is therefore employed here. Total energy convergence was found at an energy cutoff of 11 Hartree.

3.2. Optical spectra calculations

From the ground state calculations we obtain the Kohn–Sham (KS) band structure, defined by the KS-GGA eigenvalues ϵ_i, the KS-GGA wave functions ϕ_i, and the occupation numbers f_i. The KS independent-particle polarizability χ^0 is then constructed as a sum over independent transitions:

$$\chi^0(\mathbf{r}, \mathbf{r}', \omega) = \sum_{ij} 2(f_i - f_j) \frac{\phi_i^*(\mathbf{r})\phi_j(\mathbf{r})\phi_j^*(\mathbf{r}')\phi_i(\mathbf{r}')}{\omega - (\epsilon_j - \epsilon_i) + i\eta} \tag{1}$$

The factor 2 takes into account the spin degeneracy of the system.

In the case of periodic systems it can be convenient to move to the reciprocal space, where the Fourier transform of the polarizability is a matrix of the reciprocal lattice vectors $\mathbf{G}$ and $\mathbf{G}'$. The connection with measurable quantities is done through the dielectric function. In the Random Phase Approximation (RPA) the microscopic dielectric function ε is obtained via:

$$\varepsilon_{\mathbf{G},\mathbf{G}'}(\mathbf{q}) = \delta_{\mathbf{G},\mathbf{G}'} - v_{\mathbf{G}}(\mathbf{q})\chi^0_{\mathbf{G},\mathbf{G}'}(\mathbf{q}) \tag{2}$$

where v is the Coulomb interaction. For a comparison with absorption experiments one needs the macroscopic dielectric function, which is obtained by the formula due to Adler and Wiser [26–28]:

$$\varepsilon_{\mathrm{M}}(\omega) = \lim_{\mathbf{q}\to 0} \frac{1}{[\varepsilon^{-1}(\mathbf{q}, \omega)]_{\mathbf{G}=\mathbf{G}'=0}} \tag{3}$$

Neglecting the off-diagonal elements of $\varepsilon_{\mathbf{G},\mathbf{G}'}$ is equivalent, in direct space, to assume that the microscopic dielectric function $\varepsilon(\mathbf{r}, \mathbf{r}', \omega)$ does not depend explicitly on the positions $\mathbf{r}$ and $\mathbf{r}'$, but simply on the distance $\mathbf{r} - \mathbf{r}'$, as if the system were homogeneous. This assumption leads hence to a macroscopic dielectric function in the form of the spatial average of the microscopic dielectric function:

$$\varepsilon_{\mathrm{M}}(\omega) = \lim_{\mathbf{q}\to 0} \varepsilon_{\mathbf{0},\mathbf{0}}(\mathbf{q}, \omega) \tag{4}$$

For the absorption spectrum the imaginary part is taken, and for positive frequencies one obtains the usual Fermi's golden rule form

$$\Im\mathrm{m}\big(\varepsilon_{\mathrm{M}}(\omega)\big) = 2\frac{4\pi^2}{\Omega N_{\mathbf{k}}} \lim_{\mathbf{q}\to 0} \frac{1}{\mathbf{q}^2} \sum_{v,c,\mathbf{k}} \big|m_{v,c,\mathbf{k}}(\mathbf{q})\big|^2 \delta\big(\omega - (\epsilon_{c,\mathbf{k}} - \epsilon_{v,\mathbf{k}+\mathbf{q}})\big) \tag{5}$$

[1] The ABINIT code is a common project of the Universite Catholique de Louvain, Corning Incorporated, the Universite de Liege, the Commissariat a l'Energie Atomique, Mitsubishi Chemical Corp., the Ecole Polytechnique Palaiseau and other contributors (URL http://www.abinit.org).

where v denotes an occupied state and c denotes an unoccupied state. Ω is the volume of the cell and $N_{\mathbf{k}}$ the number of k-points. The matrix elements $m_{v,c,\mathbf{k}}(\mathbf{q})$ are given by $m_{v,c,\mathbf{k}}(\mathbf{q}) \equiv \langle c, \mathbf{k}|e^{-i\mathbf{qr}}|v, \mathbf{k}+\mathbf{q}\rangle$. Beyond this simplest formula, the off-diagonal terms in the dielectric matrix reflect the non-homogeneity of the space. The difference between Eq. (3) and its counterpart for an homogeneous system Eq. (4) constitutes the so-called crystal local field effect (LFE) corrections [29]. The RPA (with or without LFE) can be used for a qualitative, and sometimes quantitative, description of absorption spectra. However, in many cases (see e.g. [30] and [31]) it is necessary to go beyond this level of approximation in order to have a reliable description of the experimental spectra. Further terms have therefore to be included in the calculations. In a quasi-particle picture in the framework of MBPT, these terms stem from electron–electron and electron–hole interactions. Electron–electron interaction intervenes in the definition of quasi-particle states. The KS eigenvalues are in fact not meant to describe electron addition and removal energies for the interacting system: in fact, it is well known that KS theory systematically underestimates photoemission gaps. They can be corrected by replacing the KS equation by a corresponding quasiparticle equation within the Green's function many-body formalism. For our GeTe systems, we evaluated quasi-particle eigenvalues in the state-of-the-art Hedin's *GW* approximation (GWA) [32]. Here G represents the one particle Green's function and W the screened Coulomb potential. Now a GW-RPA optical spectrum can be calculated by replacing the GGA eigenvalues in Eq. (1) by the *GW* eigenvalues (note that the correction is evaluated to 1st order, so that the wave functions are not modified) and repeating the steps described in Eqs. (2) and (3) or (4).

The calculation of the optical gaps still needs a further correction: as in the absorption process the excited electron does not leave the system, it can interact with the hole left in the valence state and create an electron–hole pair (*exciton*). Depending on the strength of the electron–hole interaction, excitons can lead to bound states within the gap and/or to strong deformations above the continuum absorption edge. The importance of these effects depends on the screening of the electron–hole interaction and on details of the band structure and has been found to be important even for simple semiconductors like silicon [33,34]. To check the importance of excitonic effects for GeTe we have therefore solved the Bethe–Salpeter equation (BSE) for the two-particle Green's function of electron–hole pairs (see e.g. [34]). Now, transitions are mixed due to the electron–hole interaction:

$$\Im\mathrm{m}\big(\varepsilon_{\mathrm{M}}(\omega)\big) = 2\pi \lim_{\mathbf{q}\to 0} v_0(\mathbf{q}) \sum_{\lambda} \left| \sum_{vc\mathbf{k}} \big\langle v, \mathbf{k}\big|e^{-i\mathbf{q}\cdot\mathbf{r}}\big|c, \mathbf{k}+\mathbf{q}\big\rangle A_{\lambda}^{vc\mathbf{k}} \right|^2 \delta(\omega - E_{\lambda}) \tag{6}$$

The new transition energies E_λ and coefficients $A_\lambda^{vc\mathbf{k}}$ are obtained by diagonalizing a two particle electron–hole operator $H_{vc\mathbf{k}}^{v'c'\mathbf{k}'}$.[2] When no interaction is present, the Hamiltonian is diagonal ($H_{vc}^{v'c'} = (\epsilon_c - \epsilon_v)\delta_{vv'}\delta_{cc'}$) and the A_λ^{vc} are δ-functions $\delta_{v,v_\lambda}\delta_{c,c_\lambda}$: in this case, Fermi's golden rule Eq. (5) is obtained. Already when crystal LFE's are taken into account, this simple picture changes. In the language of excitons, LFE's are equivalent to an electron–hole exchange interaction (in fact, the corresponding term can be cast into the form of such an interaction term in the electron–hole Hamiltonian $H^{ex} \sim 2\int \phi_c\phi_v^*\bar{v}\phi_{c'}^*\phi_{v'}$). Here $\bar{v}$ represents the short range components of the Coulomb potential. Since H^{ex} has off-diagonal elements ($v \neq v', c \neq c'$), the A_λ^{vc} start to mix transitions. An additional mixing occurs when the electron–hole attraction is taken into account given by $H^{scr} \sim -\int \phi_c\phi_{c'}^* W\phi_v^*\phi_{v'}$. Here the screened Coulomb interaction W is the same as calculated for the *GW* approximation.[3] This has been shown to be a very good approximation for the absorption spectra of semiconductors.

Concerning convergence issues, the spectra for the crystalline phases converged when 864 off-symmetry shifted k-points in the full Brillouin zone were used to perform the summation in Eq. (1). In the optical spectra calculation 9 bands have been used. For the supercell calculations 64 shifted k-points were sufficient to reach convergence, 224 bands have been employed here in the optical spectra calculation.

4. Experimental data

The calculated absorption spectra are compared with experimental results. The experimental data are obtained by optical spectroscopy measurements of thin films of GeTe (20–500 nm) thermally evaporated on glass or Si substrates. The measurements, including Fourier Transformed Infrared (FTIR) spectroscopy and spectroscopic ellipsometry, were

[2] In the following the indices $\mathbf{k}$ and $\mathbf{k}'$ will be omitted.

[3] To be precise, Eq. (6) is an approximation that considers only the mixing of resonant transitions.

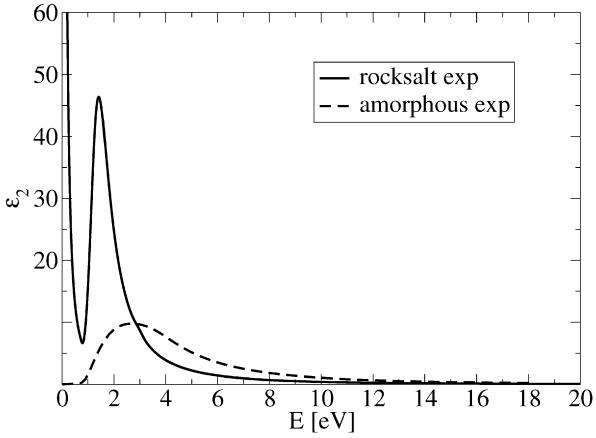

Fig. 2. Optical absorption of GeTe. Experimental data obtained by FTIR spectroscopy and ellipsometry. The data has been extrapolated up to 20 eV in order to check the sum rule.

performed in the combined energy range between 0.1 and 5.4 eV. The results shown in Fig. 2 are in line with measurements of other PCM's such as $Ge_1Sb_2Te_4$, $Ge_2Sb_2Te_5$ or $Ge_1Sb_4Te_7$ found in the literature [35,36]. It is found that the absorption spectrum in the amorphous phase is considerably flatter and broader than in the crystalline phase. Nevertheless, the f-sum rule (see e.g. [37]) is satisfied and yields similar values for both phases indicating that the two spectra are of the same quality. Regarding the comparison with the calculated spectra we would like to point out that the measured samples exhibit surfaces, grain boundaries and structural defects in both phases, which are not present in the calculated models. On top of these experimental complications the chosen model for the amorphous phase still exhibits long range order which is not present in the experiment. Therefore, we do not expect quantitative agreement between the experimental and the calculated spectra. Nevertheless we will show, that our method enables us to study qualitatively the correlation of changes in the short range atomic order as found in PCM's and changes in optical properties.

5. Calculated electronic structure in the ground state

Several articles on *ab initio* ground state calculations of crystalline GeTe can be found in the literature, e.g. [18,38]. As our results for the structural and electronic properties of the rocksalt phase agree well with these data, we only give a short summary of the results of the ground state properties of crystalline GeTe.

In the undistorted rocksalt phase the relaxed lattice parameter is found to be in very good agreement with the experimental value. The deviation between the calculated value of 6.02 Å and the experimental value of 6.01 Å [39] is less than 1%. The distorted configurations relax towards structures with short and long Ge–Te bonds similar to the bonding configuration found in the trigonal ground state structure. The total energy per atom is 24 ± 0.1 meV lower in the distorted cubic configuration, indicating that the crystalline rocksalt phase of GeTe stabilizes in a distorted configuration with short and long heteropolar bonds as already found for $Ge_1Sb_2Te_4$ [8] and $Ge_2Sb_2Te_5$ [6]. The mean deviation of the bond lengths from the bonds in the undistorted lattice (3.0 Å) corresponds to 0.22 Å.

After relaxation the three models for the amorphous phase show a volume increase of 5.1% (switch2), 7.9% (switch4.1), 8.8% (switch4.0) and 9.8% (switch8) compared to the crystalline state. This compares well with the estimation for the density decrease of 5–10% by [21] and the density decrease of 6–10% measured for ternary GeSbTe alloys [19,20]. The values for the electronic band gap of the amorphous and crystalline phases can be found in Table 1. The experimental data are extrapolated from the optical spectroscopy measurements. They suggest that the gap is similar in both phases. The Kohn–Sham gaps are -as expected- smaller than the experimental values. While in the crystalline phase the gap amounts to 0.4 eV, both in the distorted and the undistorted crystalline configuration, in the models for the amorphous phase it decreases for larger fractions of Ge atoms with tetrahedral short range order and finally vanishes for the configuration switch8. At this point we would like to mention that in the PCM $Ge_2Sb_2Te_5$ a Burstein–Moss shift [41] was found which arises from the p-type conductivity of this material due to intrinsic Ge/Sb vacancies [35] increasing the absorption edge by about 0.2 eV. Furthermore for GeTe Tsu et al. have assumed that

Table 1
Electronic band gaps for crystalline and amorphous GeTe. The calculated data are taken from the KS-GGA eigenvalues. The *GW* correction is discussed in detail in Section 6. The experimental values are extrapolated from optical spectroscopy experiments as described in Section 3.

	E_g [eV]	E_g [eV]
	amorphous	crystalline
exp	0.6	0.7
GGA		
		0.4
switch2	0.5	
switch4.0	0.1	
switch4.1	0.3	
switch8	metallic	
GW		0.55

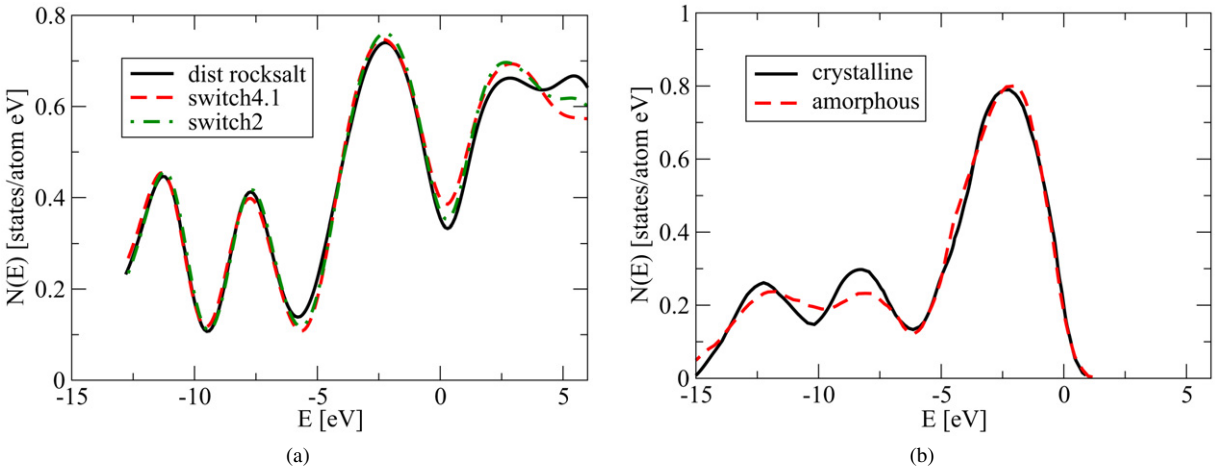

(a) (b)

Fig. 3. Photoemission spectra of crystalline and amorphous GeTe. (a) shows the calculated Electronic Density of States (DOS) for the distorted rocksalt phase and two of the models for the amorphous phase (switch2, switch4.1) from the GGA calculation. (b) shows experimental data taken from [40]. Both plots show only small differences between the two phases.

the optical absorption edge is Burstein-shifted as well [42]. Hence the band gap without Burstein–Moss amounts to ~ 0.5 eV. This is the value we would compare with theory. Although the Kohn–Sham gaps are smaller, the tendencies in the calculated and the experimental gaps should be similar. The best agreement with the tendency from the experiment – a similar gap in the crystalline and the amorphous phase – is found for the configurations switch2, and switch4.1. Furthermore these systems which only have fractions of 6.25% and 12.5% respectively of Ge atoms in tetrahedral positions exhibit a density change upon amorphization which is within the range of the experimental values. Thus the ground state calculations suggest that only a small fraction of Ge atoms switch to tetrahedral local order upon amorphization.

Fig. 3 shows a comparison of the electronic density of states (DOS) from the GGA-calculation with experimental data obtained by X-ray photoemission spectroscopy by Shevchik et al. [40]. The measured and calculated data for the occupied states agree well qualitatively. Shevchik et al. concluded that the spectrum of amorphous GeTe can be interpreted as a broadened version of that of crystalline GeTe and stated that on the other hand this is no reason to doubt that not only the long-range but also the short-range order has changed, which they inferred from changes in the dielectric constant, radial distribution functions and density. The first peak below the Fermi energy stems from the Ge 4p and Te 5p electrons, the second one from the Ge 4s electrons and the lowest in energy from the Te 5s electrons.

The calculated data reproduce the main peaks of the valence band density as well as the differences between the crystalline and the amorphous phases. In particular, we would like to point out that subtle changes as the sharpening of the largest peak in the amorphous phase which is found in the measurement and which covers the energy range of

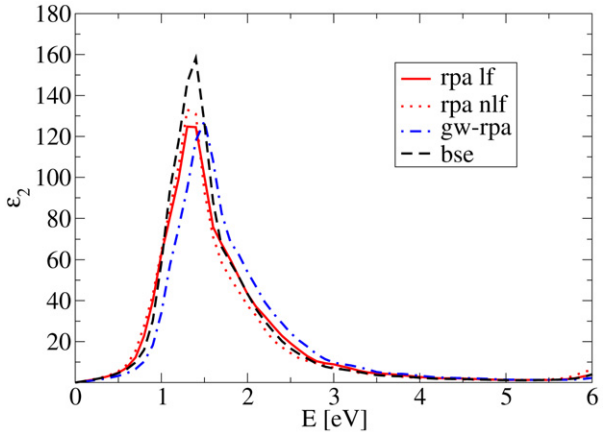

Fig. 4. Optical spectra of the undistorted rocksalt phase based on many-body perturbation theory compared to the RPA results (red full line: with crystal local fields, red dotted without crystal local fields). The GWA calculation shifts the eigenvalues 0.15 eV to higher energies, which results in a blue-shift of the absorption peak (blue dot dashed line). Taking into account excitonic effects leads to a small red-shift with respect to the GW-RPA data and to an increase of absorption strength (black dashed line). Solving the Bethe–Salpeter equation yields a negligible exciton binding energy. (For interpretation of the references to colour in this figure legend, the reader is referred to the web version of this article.)

interest for the optical spectra is correctly reproduced as well as the enhanced dip between the first and the second peak below the Fermi level. The broadening of the two small peaks in the amorphous spectrum is less pronounced than in the experiment as a simple model is used in the calculation of the amorphous phase, which still exhibits long range order. The closing of the electronic gap is due to the fact that the calculated DOS has been broadened in order to reproduce the experimental resolution of 1.5 eV. Above all the large changes of the optical properties upon amorphization are highly remarkable considering the fact that the electronic density of states of the occupied states displays only minor changes.

6. Optical properties

6.1. Results from many-body perturbation theory calculations

Here we demonstrate for the undistorted rocksalt phase of crystalline GeTe that the RPA calculations – despite their simplicity – contain all crucial features of the absorption spectra of GeTe. To do so we have to take into account electron–electron and electron–hole interactions which are not included in RPA calculations. Therefore for this system we have performed calculations based on many-body perturbation-theory to account for the underestimation of the electronic gap in DFT (electron–electron interaction) and for excitonic contributions in the absorption spectrum (electron–hole interaction). First a correction of the energies of the excited electronic states is obtained by means of a GWA calculation. To include the electron–hole interaction the Bethe–Salpeter equation is then solved (see Section 3). Fig. 4 displays a comparison of the spectra obtained with the different methods. First of all the importance of the crystal local fields, which stem from the off-diagonal elements of the matrix of the dielectric function ε and account for the spatial inhomogeneities, are studied. The RPA spectra obtained by the *dp*-code [43] including local fields (rpa lf) and not including them (rpa nlf) do not differ substantially (nevertheless crystal local fields are taken into account in the subsequent spectra presented in this article). The eigenvalues obtained from the GWA calculated by the *abinit*-code (see footnote 1) are shifted to higher energies by 0.15 eV compared to the GGA eigenvalues. Thus the *GW* calculation results in a minor correction of the electronic structure (gw-rpa) towards the experimental value.

The electron–hole interaction in the BSE absorption spectrum (calculated by the *exc*-code [44]) cancels the *GW* blue shift and moves the absorption peak back to the RPA position. This is due to a redistribution of the oscillator strength of the optical transitions. Therefore, the net result of the many body effects is only a modest increase of the peak height. However, no significant features which are absent in the RPA spectrum additionally appear if we include excitonic effects in our simulations. Therefore one can conclude that many body contributions are rather small and that the RPA spectra include all crucial features in the absorption spectrum of GeTe. This is due to the strong screening

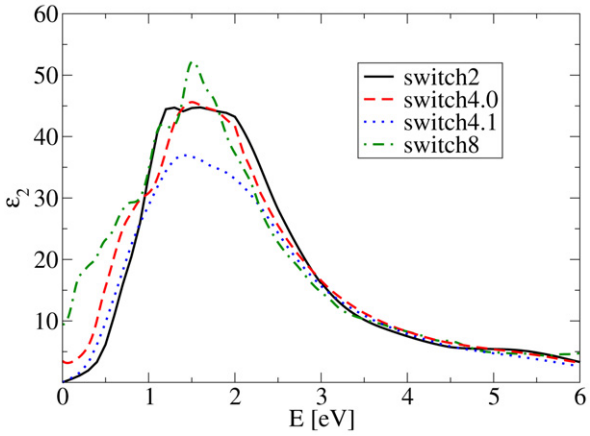

Fig. 5. Absorption spectra of the models for the short range order in the amorphous phase of GeTe. Except for the absorption of switch8, which is more structured the spectra are similar. Switch4.1 features a weaker absorption peak than the other systems.

found in the system. Experimentally, a value of 36 for the electronic dielectric constant is obtained for the trigonal ground state [42,45]. A further reduction of many-body effects in the system is induced by lattice polarization and the free carriers present in the experimental probes. Thus in the following it is sufficient to consider the RPA spectra to study the correlations between the short range order and the optical properties as proposed in [17].

6.2. The optical spectra of different amorphous configurations

Fig. 5 shows the calculated RPA absorption spectra for the four models of the amorphous short range order. The general shape of the spectra is very similar. They all exhibit one absorption peak, which is broader and lower than in the crystalline phase. For the model switch4.1 the peak intensity is considerably weaker compared to the other models. In particular the difference between the spectra of the two models switch4.0 and switch4.1 shows the importance of the local structure. Further differences are established in the slightly more structured shape of the absorption peak belonging to switch8 and the different onsets of the absorption which are due to the different band gap values in the four models. However, we can conclude that the overall shape and position of the absorption in the amorphous phase does not strongly depend on the number of Ge atoms which change from sixfold to fourfold coordination. As the tendency for the electronic gap agrees best with the experimental data (see Table 1) for switch4.1, we use this model for the further analysis.

6.3. Distortions and defects in the crystalline phase

For the crystalline phase the electronic properties are calculated in the distorted and in the undistorted structure and compared with experimental data. Fig. 6 shows the imaginary part of the dielectric function derived from the RPA calculations and the experiment. In contrast to the spectra labeled “undist. rpa” and “dist. rpa” the experimental absorption spectrum exhibits a peak at energies below 0.5 eV. This peak stems from Ge vacancies which are known to be the dominant point defects in crystalline GeTe (see e.g. [46]). They induce unoccupied states at the valence band edge resulting in p-type conductivity [42,47] with a reported charge carrier density 3×10^{20} cm^{-3} and 13×10^{20} cm^{-3} [48]. This conductivity gives rise to the Drude peak observed in the experimental absorption spectrum and to a Burstein–Moss shift of the absorption edge. In fact the Drude peak is found in the calculated spectrum if a Ge-vacancy is included in the supercell (undist. vac. rpa). Furthermore the Burstein–Moss shift eliminates transitions at the valence band edge and thus might be responsible for the decrease in the absorption strength observed when comparing the system with and without vacancies. As we do not intend to study the defect properties in GeTe but rather the correlation between the short-range order and the optical properties, we will not consider these point defects in the following discussion.

The experimental absorption spectrum exhibits a lower peak intensity than the calculated ones. However in our calculations the distorted crystalline structure exhibits better agreement with the experimental data for both the ab-

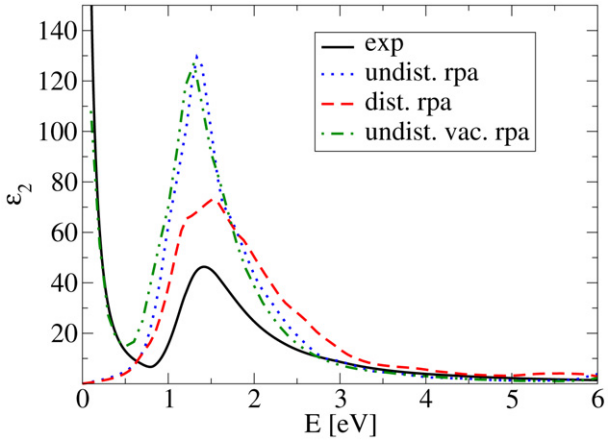

Fig. 6. Optical absorption in the crystalline rocksalt phase of GeTe from the calculation and the experiment. The spectrum of the distorted system (dist. rpa) agrees better with the experiment (exp) than the spectrum of the undistorted system (undist. rpa). The Drude peak of the experimental spectrum is reproduced by creating a Ge-vacancy in the calculated undistorted system.

sorption intensity and the peak shape of the absorption. Furthermore we find good qualitative agreement for the peak position and asymmetric shape of the calculated and the experimental spectra, despite using RPA. The comparison between the spectra of the distorted and the undistorted model shows, that the distortions play a significant role for the absorption in crystalline GeTe. Evidently PCM's without or with fewer distortions will exhibit a stronger absorption in the crystalline phase and hence a larger optical contrast with the amorphous phase. As it is possible to control the degree of the distortions in PCM's by changing the stoichiometry [16], this is an important result for the application of PCM's in optical data storage.

6.4. Comparison with experimental data

Fig. 7 shows the RPA absorption spectra for the distorted rocksalt model and the amorphous model switch4.1 (a) compared with the experimental data (b). Qualitative agreement is found in the spectra and the trends observed in the experiment are well reproduced by the calculations: The absorption decreases and broadens in the amorphous phase. Intuitively one might assume that upon amorphization the electronic density of states (DOS) broadens as the reduction of structural symmetries also lifts the degeneracies for the electronic states. This consequently gives rise to a broader and flatter absorption spectrum compared with the crystalline phase. However, as the model for the amorphous phase exhibits long range order, this decrease and broadening in the RPA spectra does not stem from a smearing and broadening of the electronic density of states caused by the lack of long range order. Therefore it must originate from the change in short range atomic order.

To reveal the origin of the difference in optical absorption between the amorphous and the crystalline phase as well as between the distorted and the perfect rocksalt systems it is studied whether this difference is related to a change of the matrix elements or to a change of the band structure. To do so, we first approximate the matrix elements of the optical transitions. In fact in the dipole approximation one obtains

$$\langle c, \mathbf{k}-\mathbf{q}|e^{-i\mathbf{q}\cdot\mathbf{r}}|v, \mathbf{k}\rangle \sim \frac{\langle c, \mathbf{k}|i\mathbf{q}[\mathbf{r}, H]|v, \mathbf{k}\rangle}{\epsilon_{c,\mathbf{k}} - \epsilon_{v,\mathbf{k}}} \tag{7}$$

Thus Eq. (5) becomes

$$\begin{aligned}\Im\mathfrak{m}\big(\varepsilon_M(\omega)\big) &= 2\frac{4\pi^2}{\Omega N_{\mathbf{k}}} \lim_{\mathbf{q}\to 0} \frac{1}{\mathbf{q}^2} \sum_{vc\mathbf{k}} \frac{|\langle c, \mathbf{k}|i\mathbf{q}[\mathbf{r}, H]|v, \mathbf{k}\rangle|^2}{(\epsilon_{c,\mathbf{k}} - \epsilon_{v,\mathbf{k}})^2} \delta\big(\omega - (\epsilon_{c,\mathbf{k}} - \epsilon_{v,\mathbf{k}})\big) \\ &= 2\frac{4\pi^2}{\Omega N_{\mathbf{k}}\omega^2} \lim_{\mathbf{q}\to 0} \frac{1}{\mathbf{q}^2} \sum_{vc\mathbf{k}} \big|\langle c, \mathbf{k}|i\mathbf{q}[\mathbf{r}, H]|v, \mathbf{k}\rangle\big|^2 \delta\big(\omega - (\epsilon_{c,\mathbf{k}} - \epsilon_{v,\mathbf{k}})\big)\end{aligned} \tag{8}$$

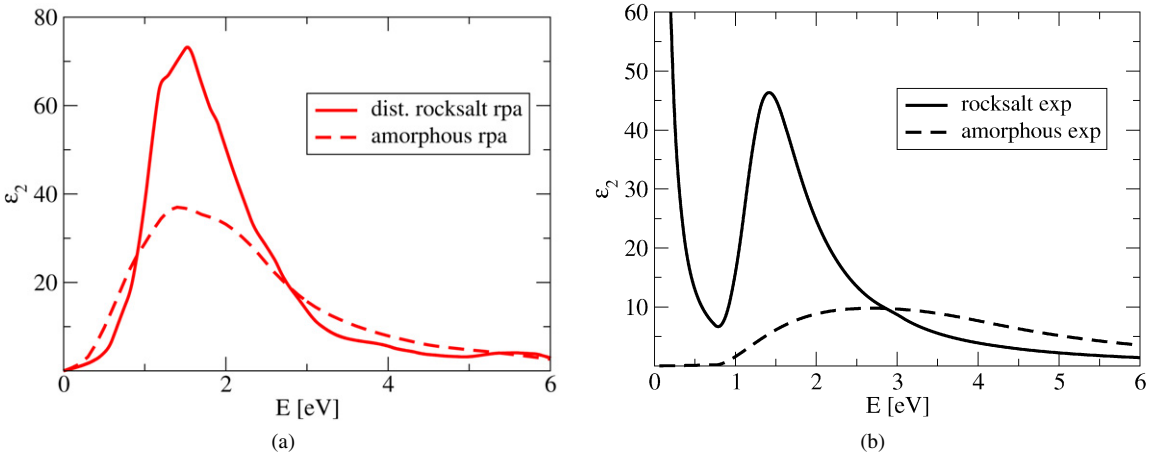

Fig. 7. Optical absorption of GeTe: The calculations (a) predict stronger absorption for crystalline and amorphous bulk GeTe than found in optical spectroscopy of thin GeTe films (b). The trend upon amorphization is nevertheless reproduced: The absorption decreases and broadens in the amorphous phase, in the RPA calculations as well as in the experiment.

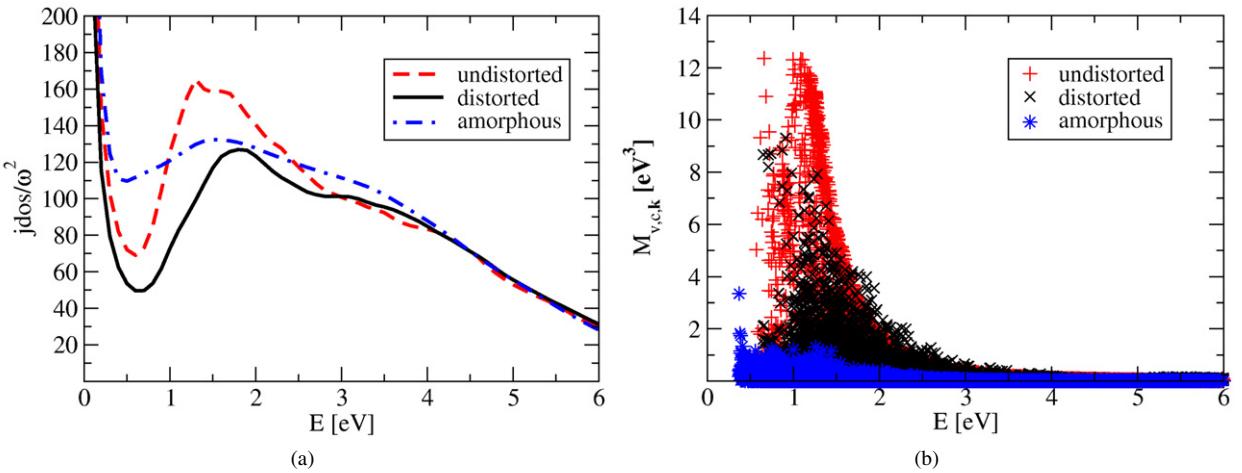

Fig. 8. (a) The JDOS/ω^2 of the distorted and undistorted crystalline state and of the amorphous state of GeTe in number of transitions/eV^3 per cell and k-point. Up to 1.7 eV more transitions are found in the undistorted phase. (b) The matrix elements $M_{v,c,\mathbf{k}} = 2\frac{4\pi^2}{\Omega}\lim_{\mathbf{q}\to 0}\frac{1}{\mathbf{q}^2}|\langle c\mathbf{k}|i\mathbf{q}[\mathbf{r}, H]|v\mathbf{k}\rangle|^2$ in the distorted and undistorted crystalline state and of the amorphous state in arbitrary units. Both the JDOS and the matrix elements show differences between the undistorted and the distorted crystalline structure as well as between the crystalline and the amorphous states.

Now one can define the joint density of states (JDOS) as

$$\frac{JDOS}{\omega^2} \equiv \frac{1}{N_{\mathbf{k}}\omega^2}\sum_{v,c,\mathbf{k}}\delta(\epsilon_{c,\mathbf{k}} - \epsilon_{v,\mathbf{k}} - \omega) \tag{9}$$

Fig. 8 shows the JDOS/ω^2 (a) and the matrix elements (b) of the distorted and the undistorted cubic system and of the model for the amorphous phase (switch4.1). As reported in [17] the difference between the spectra in the crystalline and the amorphous phase is due to a change in the oscillator strength of the optical transitions. Up to 1.7 eV more transitions are found in the JDOS of the amorphous phase. The change in the absorption spectrum upon amorphization thus cannot be solely understood as a change of the band structure. On the other hand, weaker matrix elements are found in the amorphous phase explaining the strong decrease of the optical absorption upon amorphization. Concerning the two crystalline phases, the differences in the absorption spectra can be attributed to both, a change in the JDOS as well as to a change in the matrix elements. Both show differences between the two

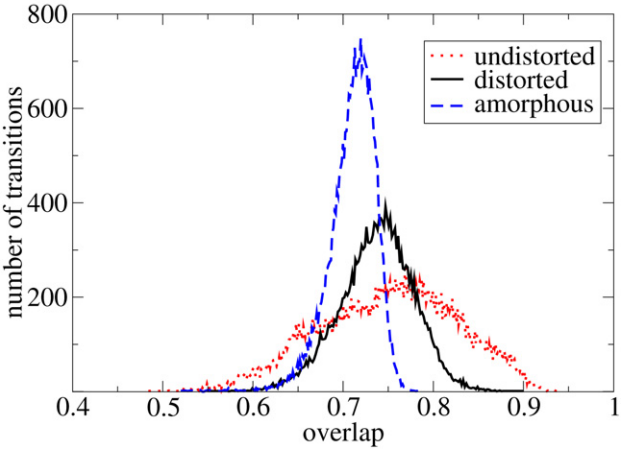

Fig. 9. The number of matrix elements for excitation energies up to 2.5 eV plotted against the overlap $\int |\phi_c(\mathbf{r})||\phi_v(\mathbf{r})|\,\mathrm{d}\mathbf{r}$ of the wave functions in the distorted, undistorted and in the amorphous phase. Upon distorting the crystal the overlap decreases significantly.

phases and thus contribute to the decrease of the optical absorption which is observed upon distorting the perfect rocksalt lattice. The effect of the matrix element is not as pronounced for the phase transition between the crystalline and the amorphous phase but nevertheless it cannot be neglected.

Similar to the change of the matrix elements between the distorted crystalline and the amorphous phase shown in [17], the change between the distorted and the undistorted crystalline phase can be attributed to a change of the overlap of the wave functions involved in the optical transitions. Fig. 9 shows the number of matrix elements plotted against the overlap $\int |\phi_c(\mathbf{r})||\phi_v(\mathbf{r})|\,\mathrm{d}\mathbf{r}$ in the two crystalline phases and in the amorphous phase. In the distorted phase the weight of the curve slightly shifts towards lower values indicating a weaker overlap between the wave functions compared to the undistorted phase. This decrease of the overlap explains the decrease of the matrix elements, which is the origin of the change in optical properties. This effect again reveals the importance of the local atomic order in PCM's for their optical properties.

7. Conclusions

In this work we have employed *ab initio* calculations to study the optical properties in the PCM GeTe in the crystalline and the amorphous phases. Electronic ground state calculations have been performed to establish the structural models. It is found that the crystalline rocksalt structure of GeTe exhibits local distortions which lead to the formation of short and long bonds in the system. Similar distortions recently have been found for GeSbTe alloys [8,6]. Furthermore we have constructed a model of the amorphous phase of GeTe based on recent experimental observation that Ge atoms change their local bonding configuration upon amorphization [6–8]. A comparison of the electronic structure, namely the electronic gap with experimental results provide good results if only a small fraction of Ge atoms (between 6%–12%) changes the bonding configuration from sixfold to fourfold coordination. The calculated DOS of the crystalline structure and of the models for the amorphous phase agree well with experimental data.

The optical spectra calculations yield several important results and lead to a better understanding of the optical properties in PCM's. To confirm the validity of the RPA results presented in [17] we have performed calculations based on many-body perturbation theory in the crystalline state. The *GW* results indicate, that due to the large screening in GeTe the electronic gap is not significantly changed with respect to the GGA calculations. The BSE spectra exhibit a rather small excitonic contribution which results in an increase of the absorption intensity. This small contribution is negligible in order to qualitatively understand the correlation between short range order and optical properties in PCM's. Thus it is sufficient to use the RPA to study the optical properties of PCM's.

The calculations of the amorphous models reveal, that it is sufficient to change the coordination of only a small fraction of Ge atoms to achieve a change in optical absorption and a density change which is in line with the experimental data. Furthermore the differences between the models switch4.0 and switch4.1 show that the precise local geometry plays an important role for the optical properties.

Finally, the role of the short-range order changes upon amorphization and of the distortions in the crystalline phase has been studied in detail. The calculations show that the optical contrast between crystalline and amorphous state is mainly due to a decrease of the matrix elements of the optical transitions upon amorphization. Furthermore, the absorption spectrum of the distorted crystalline system agrees significantly better with the experimental data than the spectrum of the undistorted system. It is observed that the absorption peak decreases in the distorted phase. Further analysis reveals, that this decrease is due to significant changes in the JDOS and the matrix elements. This impact of the distortions on the optical properties should be significant for the application of PCM's in optical data storage. As the scale of the distortions can be tuned by varying the stoichiometry [16], it is possible to adjust the optical contrast between the crystalline and the amorphous phase by a systematic modification of the stoichiometry.

Acknowledgements

This work was funded in part by the EU's 7th Framework Program through the NANOQUANTA Network of Excellence. Furthermore, W. Wełnic thanks for support from the European Community program "Marie Curie Host Fellowship" (contract number HPMT-CT-2001-00368) and the Feodor-Lynen program of the Alexander von Humboldt-Foundation.

References

[1] J. Stuke, G. Zimmerer, Phys. Stat. Sol. B – Basic Research 49 (2) (1972) 513.
[2] H.R. Philipp, H. Ehrenreich, Phys. Rev. 129 (4) (1963) 1550.
[3] J. Tauc, Amorphous and Liquid Semiconductors, Plenum Press, London, 1974.
[4] M.C. Ridgway, C.J. Glover, G.J. Foran, K.M. Yu, J. Appl. Phys. 83 (1998) 4610.
[5] W. Zachariasen, J. Am. Chem Soc. 54 (1932) 3841.
[6] A. Kolobov, P. Fons, A. Frenkel, A. Ankudinov, J. Tominaga, T. Uruga, Nature Materials 3 (2004) 703.
[7] A. Kolobov, P. Fons, J. Tominaga, A. Ankudinov, S. Yannopoulos, K. Andrikopoulos, J. Phys.: Condens. Matter 16 (2004) S5103.
[8] W. Wełnic, A. Pamungkas, R. Detemple, C. Steimer, S. Blügel, M. Wuttig, Nature Materials 5 (2006) 56.
[9] P. Jóvári, I. Kaban, J. Steiner, B. Beuneu, A. Schöps, M.A. Webb, Phys. Rev. B 77 (2008) 035202.
[10] D.A. Baker, M.A. Paesler, G. Lucovsky, S.C. Agarwal, P.C. Taylor2, Phys. Rev. Lett. 96 (2006) 255501.
[11] J. Akola, R.O. Jones, Phys. Rev. B 76 (2007) 235201.
[12] S. Caravati, M. Bernasconi, T.D. Kühne, M. Krack, M. Parrinello, Appl. Phys. Lett. 91 (2007) 171906.
[13] S.R. Ovshinsky, Phys. Rev. Lett. 21 (1968) 1450.
[14] M. Libera, M. Chen, J. Appl. Phys. 73 (1993) 2272.
[15] N. Yamada, MRS Bull. 21 (9) (1996) 48.
[16] M. Wuttig, D. Lüsebrink, D. Wamwangi, W. Wełnic, M. Gilleßen, R. Dronskowski, Nature Materials 6 (2007) 122.
[17] W. Welnic, S. Botti, L. Reining, M. Wuttig, Phys. Rev. Lett. 98 (2007) 236403.
[18] K.M. Rabe, J.D. Joannopoulos, Phys. Rev. B 36 (1987) 6631.
[19] V. Weidenhof, I. Friedrich, S. Ziegler, M. Wuttig, J. Appl. Phys. 86 (10) (1999) 5879.
[20] D. Wamwangi, W. Njoroge, M. Wuttig, Thin Solid Films 408 (2002) 310.
[21] W.E. Howard, R. Tsu, Phys. Rev. B 1 (1970) 4709.
[22] X. Gonze, J. Beuken, R. Caracas, F. Detraux, M. Fuchs, G. Rignanese, L. Sindic, M. Verstraete, G. Zerah, F. Jollet, M. Torrent, A. Roy, M. Mikami, P. Ghosez, J. Raty, D. Allan, Comput. Mater. Sci. 25 (2002) 478.
[23] M. Fuchs, M. Scheffler, Comput. Phys. Commun. 119 (1) (1999) 67.
[24] J.P. Perdew, K. Burke, M. Ernzerhof, Phys. Rev. Lett. 77 (18) (1996) 3865.
[25] G. Makov, R. Shah, M.C. Payne, Phys. Rev. B 53 (1996) 15513.
[26] S.L. Adler, Phys. Rev. 126 (1962) 413.
[27] N. Wiser, Phys. Rev. 129 (1963) 62.
[28] H. Ehrenreich, in: J. Tauc (Ed.), The Optical Properties of Solids, Proceedings of the International School of Physics "Enrico Fermi", Academic, New York, 1966, p. 106, course XXXIV.
[29] S. Baroni, R. Resta, Phys. Rev. B 33 (1986) 7017, and references therein.
[30] G. Onida, L. Reining, A. Rubio, Rev. Mod. Phys. 74 (2002) 601.
[31] S. Botti, A. Schindlmayr, R. Del Sole, L. Reining, Rep. Prog. Phys. 70 (2007) 357–407.
[32] L. Hedin, Phys. Rev. A 139 (1965) 796.
[33] W. Hanke, L.J. Sham, Phys. Rev. Lett. 43 (1979) 387.
[34] S. Albrecht, L. Reining, R.D. Sole, G. Onida, Phys. Rev. Lett. 80 (1998) 4510.
[35] B.S. Lee, J.R. Abelson, S.G. Bishop, D.H. Kang, B.K. Cheong, K.B. Kim, J. Appl. Phys. 97 (2005) 093509.
[36] E. Garcia-Garcia, A. Mendoza-Galvan, Y. Vorobiev, E. Morales-Sanchez, J. Gonzalez-Hernandez, G. Martinez, B. Chao, J. Vacuum, Sciences & Technology A – Vacuum Surfaces and Thin Films 17 (1999) 1805.
[37] M.H. Brodsky, P.J. Stiles, Phys. Rev. Lett. 25 (1970) 798.

[38] Y.W. Tung, M.L. Cohen, Phys. Rev. 180 (3) (1969) 823.
[39] J.N. Bierly, L. Muldawer, O. Beckman, Acta Metall. 11 (1963) 447.
[40] N. Shevchik, J. Tejeda, D. Langer, M. Cardona, Phys. Rev. Lett. 30 (14) (1973) 659.
[41] T. Moss, Optical Properties of Semi-Conductors, Butterworth, London, 1959.
[42] R. Tsu, W.E. Howard, L. Esaki, Phys. Rev. 172 (1968) 779.
[43] V. Olevano, L. Reining, F. Sottile, http://www.dp-code.org.
[44] http://www.bethe-salpeter.org.
[45] S.K. Bahl, K.L. Chopra, J. Appl. Phys. 40 (1969) 4940.
[46] A.V. Kolobov, J. Tominaga, P. Fons, T. Uruga, Appl. Phys. Lett. 82 (3) (2003) 382.
[47] A.H. Edwards, A.C. Pineda, P.A. Schultz, M.G. Martin, A.P. Thompson, H.P. Hjalmarson, C.J. Umrigar, Phys. Rev. B 73 (2006) 045210.
[48] N. Kolomoets, B. Lev, L. Sysoeva, Sov. Phys. Solid State 6 (1964) 551.